Topological edge states of the $\mathcal{PT}$-symmetric Su-Schrieffer-Heeger model: An effective two-state description

A. F. Tzortzakakis [1,2] A. Katsaris [2] N. E. Palaiodimopoulos [1] P. A. Kalozoumis [3] G. Theocharis [4] F. K. Diakonos [2] and D. Petrosyan [1,5]

[1] *Institute of Electronic Structure and Laser, FORTH, GR-70013 Heraklion, Crete, Greece*
[2] *Department of Physics, National and Kapodistrian University of Athens, GR-15784 Athens, Greece*
[3] *Department of Engineering and Informatics, Hellenic American University, 436 Amherst Street, Nashua, New Hampshire 03063, USA*
[4] *LAUM, CNRS, Le Mans Université, Avenue Olivier Messiaen, 72085 Le Mans, France*
[5] *A. Alikhanyan National Science Laboratory (YerPhI), 0036 Yerevan, Armenia*

(Received 29 April 2022; accepted 2 August 2022; published 16 August 2022)

We consider the non-Hermitian, parity-time- [($\mathcal{PT}$)-] symmetric extensions of the one-dimensional Su-Schrieffer-Heeger model in the topological nontrivial configuration. We study the properties of the topologically protected edge states and develop an effective two-state analytical description of the system that accurately predicts the $\mathcal{PT}$-symmetry-breaking point for the edge states. We verify our analytical results by exact numerical calculations.

DOI: 10.1103/PhysRevA.106.023513

I. INTRODUCTION

Following the discovery of the quantum Hall effect, the notion of topological order was used extensively as a new criterion for classifying distinct quantum phases of matter [1–3]. One of the most significant achievements in this field was the prediction and observation of topological insulators—electronic materials that support conducting states localized on their surface or edges despite being insulating in their interior due to the existence of a bulk energy gap [4,5]. This property is a consequence of the combined effect of topological order and symmetry protection which provides extraordinary robustness to disorder and external perturbations. Topological insulators are of fundamental importance and practical significance for various potential applications, such as high-performance electronic and robust spintronic devices, protection from decoherence in quantum computing, etc. [6–9].

Recently, an optical counterpart of topological insulators was proposed [10,11] and realized [12] using photonic devices. The classical nature of optical platforms makes experimental observation and manipulation of electromagnetic waves substantially easier, preserving at the same time most of the engaging physics related to topology and symmetry protection. This extension then offers new perspectives in the broad field of topological physics [13–15].

In the meantime, another symmetry-based phenomenon—that of parity-time- [($\mathcal{PT}$)-] symmetry and exceptional points—has attracted much attention in optical physics [16–20]. Specifically, it was recently realized that optical amplification (gain) and dissipation (loss) can be employed to implement complex potentials and explore the counterintuitive physics of non-Hermitian effects. If, in addition, this optical gain and loss is incorporated in a balanced antisymmetric manner that respects $\mathcal{PT}$ symmetry, the corresponding system can possess completely real spectrum despite being non-Hermitian [21]. Then, by fine-tuning the gain-loss contrast, one can actualize spontaneous $\mathcal{PT}$-symmetry breaking in the system, whereby its eigenvalues coalesce into exceptional points (non-Hermitian degeneracies) and turn from real to complex.

It is then natural to combine the two effects and explore their interplay. Due to their seemingly contradictory character with topology inherently related to robustness and non-Hermiticity and exceptional points to extreme sensitivity, it was initially debated whether the two phenomena could coexist [22–24]. But recent theoretical and experimental studies have shown that the combined effect of topology and non-Hermiticity yields an even more exotic and unexpected physical behavior [25–34], featuring non-Hermitian topological light funneling [35] and steering [36] as well as topological lasing [37–39].

The simplest system where $\mathcal{PT}$ symmetry and topology can coexist is the Su-Schrieffer-Heeger (SSH) model with alternating gain and loss on the neighboring lattice sites. In the topologically nontrivial configuration, the SSH model possesses zero-energy edge states that are robust with respect to lattice disorder. But in any experimental realization of the model, the finite size of the lattice leads to the coupling of the edge states, and thereby to their splitting, which is now sensitive to lattice disorder. It was then suggested to use non-Hermitian degeneracies to recover the exact zero-energy modes at or beyond the critical value of the gain and loss, which was experimentally confirmed using a lattice of lossy silicon waveguides [31]. Hence, paradoxically, the $\mathcal{PT}$-symmetry breaking can strengthen the topologically protected characteristics of the edge states in finite SSH lattices.

In this paper, we focus on the properties of the edge states of the $\mathcal{PT}$-symmetric SSH model. Using an appropriate ansatz for the edge-state wave functions, we derive an

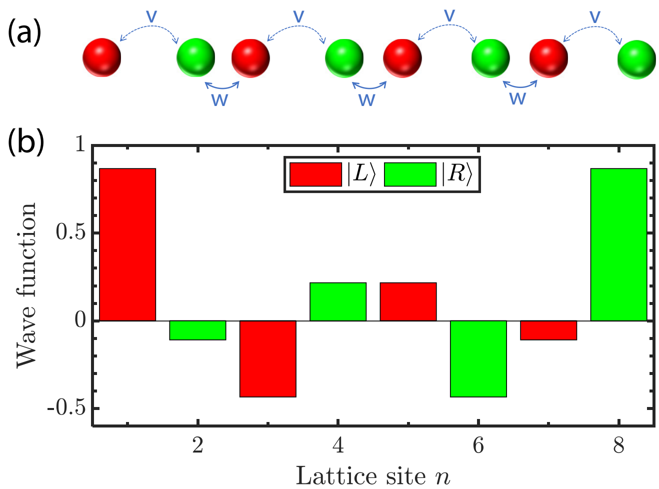

FIG. 1. (a) Schematic of a SSH lattice of $N = 8$ sites (four unit cells) with alternating nearest-neighbor couplings $v < w$ (topologically nontrivial configuration) as described by Hamiltonian (1). (b) Wave-function profiles of the ansatz edge states $|L, R\rangle$ of Eqs. (7) for $u = v/w = 0.5$

effective two-state model Hamiltonian that includes the coupling between the edge states and their (complex) energies. This model then leads to approximate analytical expressions for the values of the gain-loss contrast at the $\mathcal{PT}$-symmetry-breaking (exceptional) point of the edge-state eigenvalues at zero energy. We also show that, under appropriate conditions, our effective description can accurately predict the exceptional points for a large variety of non-Hermitian potentials as long as they respect the basic symmetries of the model and retain its bulk gap open. In all cases, we verify our analytical results with exact numerical calculations and discuss the extent of validity of our approach.

We note the earlier relevant studies of the $\mathcal{PT}$-symmetry-breaking threshold for impurity- or disorder-localized modes in a lattice [40] or in open and closed chains of dispersive waveguides with different geometries of gain and loss [41] and the existence and stability of stationary modes in $\mathcal{PT}$-symmetric arrays of nonlinear oscillators [42].

The paper is organized as follows. In Sec. II we review the properties of the Hermitian SSH model focusing on its topological edge states. In Sec III we study the $\mathcal{PT}$-symmetric SSH model with uniform gain-loss contrast, derive the effective edge-state Hamiltonian and compare its analytical predictions for the exceptional-point position and edge-state wave functions with exact numerical calculations. In Sec. IV we generalize our approach to a SSH model with spatially inhomogeneous but globally $\mathcal{PT}$-symmetric gain-loss contrast. Our conclusions are summarized in Sec. V.

II. HERMITIAN SSH MODEL

We consider a one-dimensional lattice of N (even) sites with staggered hopping amplitudes $v, w \geqslant 0$ between the neighboring sites. The system, thus, consists of two sublattices forming $N/2$ unit cellsas shown in Fig. 1(a). The "single-particle" Hamiltonian of the system is

$$\mathcal{H} = v \sum_{n_{\text{odd}}=1}^{N-1} [|n\rangle\langle n+1| + \text{H.c.}] + w \sum_{n_{\text{even}}=2}^{N-2} [|n\rangle\langle n+1| + \text{H.c.}]. \tag{1}$$

Since sites of each sublattice are coupled only with sites of the other sublattice, the system possesses chiral (sublattice) symmetry. This symmetry is formally represented by the operator $\Sigma_z \equiv \mathbb{1}_{N/2} \otimes \sigma_z$, where $\mathbb{1}_{N/2}$ is the $N/2 \times N/2$ identity operator, and σ_z is the Pauli matrix for a unit cell. Due to the chiral symmetry, this operator anticommutes with the Hamiltonian $\{\Sigma_z, \mathcal{H}\} = 0$, leading to a spectrum symmetric around zero $E \to -E$.

A. Bulk states

The bulk k-space Hamiltonian of the system is

$$\mathcal{H}(k) = \begin{pmatrix} 0 & v + we^{-ik} \\ v + we^{ik} & 0 \end{pmatrix} \equiv \begin{pmatrix} 0 & h(k) \\ h^*(k) & 0 \end{pmatrix}, \tag{2}$$

which yields the dispersion relation,

$$E(k) = \pm |h(k)| = \pm\sqrt{v^2 + w^2 + 2vw\cos k} \tag{3}$$

for a pair of bands with an energy gap $E_g = 2|v - w|$. It has been shown that the topological invariant of the SSH model is a winding number [23],

$$\mathcal{W} = \frac{1}{2\pi i}\int_{-\pi}^{\pi} dk \frac{d}{dk}\ln h(k) = \frac{1}{2\pi i}\oint_{|z|=1}\frac{dz}{v/w + z}. \tag{4}$$

It then follows from the Cauchy's integral theorem that the ratio $u \equiv v/w$ determines the topological properties of the system: for $u < 1$ the winding number is nonzero ($\mathcal{W} = 1$), and the system is topologically nontrivial, possessing zero-energy topologically protected edge states, whereas for $u > 1$ the system is topologically trivial ($\mathcal{W} = 0$), and all the states are the bulk states in the two bands with the positive and negative energies. At $u = 1$ ($v = w$) the gap vanishes and the spectrum reduces to that of a uniform lattice $E(k) = -2w\cos k/2$ ($k \in [-2\pi, 2\pi]$).

B. Edge states

We now assume the topologically nontrivial regime $u < 1$ and consider the two edge states. Following the analysis in Refs. [43–46], we present an effective description of the edge states that will be used in the following sections. In the thermodynamic limit, the left $|L\rangle$ and right $|R\rangle$ edge states are zero-energy eigenstates of the Hamiltonian,

$$\mathcal{H}|L, R\rangle = 0 \quad (N \to \infty). \tag{5}$$

Substituting here the Hamiltonian (1), we obtain simple recurrence relations for the amplitudes $c_n^{L,R}$ of the wave-functions $|L, R\rangle = \sum_n c_n^{L,R}|n\rangle$ as

$$c_{n+2}^{L,R} = -uc_n^{L,R} \quad (n \text{ odd}), \tag{6a}$$

$$c_n^{R,L} = -uc_{n+2}^{R,L} \quad (n \text{ even}). \tag{6b}$$

Assuming that $|L\rangle$ has support only on the odd sublattice sites ($c_n^L = 0\ \forall\, n$ even), and $|R\rangle$ has support only on the even sublattice sites ($c_n^R = 0\ \forall\, n$ odd), relations (6) result in the wave functions,

$$|L\rangle = c_1^L \sum_{n_{\text{odd}}=1}^{N-1} (-u)^{(n-1)/2}\, |n\rangle\,, \tag{7a}$$

$$|R\rangle = c_N^R \sum_{n_{\text{even}}=2}^{N} (-u)^{(N-n)/2}\, |n\rangle\,, \tag{7b}$$

where the normalized amplitudes are given by

$$\left|c_1^L\right|^2 = \left|c_N^R\right|^2 = \frac{1-u^2}{1-u^N}, \tag{8}$$

and, for simplicity, can be assumed real. Even though for any finite system the states in Eq. (7) are not exact eigenstates of Hamiltonian (1), they still approximate well the exact edge states especially for sufficiently small $u < 1$ and large $N \gg 1$. In Fig. 1(b) we show the wave functions of states $|L, R\rangle$ which are exponentially localized at the edges of the lattice with a localization length $\xi = -2/\ln(u)$ (see below).

Since the energies of the edge states $|L, R\rangle$ lie in the middle of the gap between the two bands, their interaction with the bulk eigenstates can be neglected. We can then write an effective two-state Hamiltonian for the edge states as

$$\mathcal{H}^{(\text{eff})} = \begin{pmatrix} \langle L|\mathcal{H}|L\rangle & \langle L|\mathcal{H}|R\rangle \\ \langle R|\mathcal{H}|L\rangle & \langle R|\mathcal{H}|R\rangle \end{pmatrix} \equiv \begin{pmatrix} \mathcal{E}_L & C \\ C^* & \mathcal{E}_R \end{pmatrix}, \tag{9}$$

where the diagonal elements represent the energies $\mathcal{E}_{L,R}$ of the edge-states $|L, R\rangle$ whereas the off-diagonal elements are their coupling C. To evaluate the matrix elements of $\mathcal{H}^{(\text{eff})}$, we first calculate the action of $\mathcal{H}$ onto the states $|L, R\rangle$ of Eq. (7),

$$\mathcal{H}\,|L\rangle = v c_1^L (-u)^{(N/2-1)}\, |N\rangle\,,$$
$$\mathcal{H}\,|R\rangle = v c_N^R (-u)^{(N/2-1)}\, |1\rangle\,.$$

Since $|L\rangle$ and $|R\rangle$ have support only on the odd and even lattice sites, respectively, we immediately obtain

$$\mathcal{E}_L = \mathcal{E}_R = 0, \quad C = v\,\frac{1-u^2}{1-u^N}(-u)^{(N/2-1)}. \tag{10}$$

For $u < 1$ and $N \gg 1$, the effective coupling between the two edge states can be approximated by

$$|C| \simeq C_0\, e^{-N/\xi}\,, \tag{11}$$

where $C_0 = \frac{w^2-v^2}{w}$ and $\xi = 2/\ln(w/v)$, which implies that the coupling falls off exponentially with N with a characteristic length ξ which coincides with the localization length of the two edge states. This coupling is also responsible for the hybridization of the two edge states in finite systems. The hybridized states are the eigenstates of the effective Hamiltonian, $\mathcal{H}^{(\text{eff})}\,|\pm\rangle = E_\pm\,|\pm\rangle$, given by the symmetric and antisymmetric superpositions of the two edge states,

$$|\pm\rangle = \frac{1}{\sqrt{2}}(|L\rangle \pm |R\rangle), \tag{12}$$

with the eigenenergies $E_\pm = \pm|C|$ that tend to zero in the limit of a long chain $N \gg \xi$.

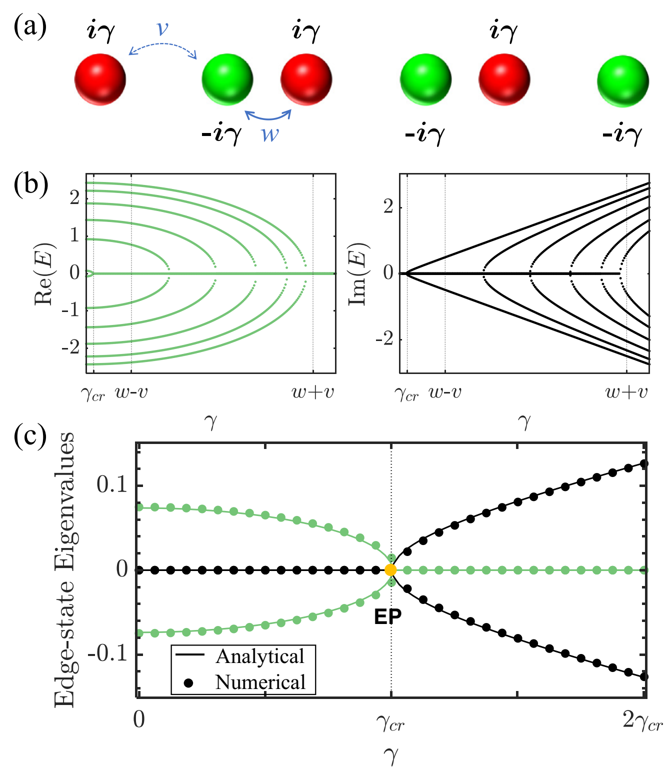

FIG. 2. (a) Schematic of a $\mathcal{PT}$-symmetric SSH chain with the nearest-neighbor couplings $v < w$ and alternating gain and loss $\pm i\gamma$ [cf. Hamiltonian (13)]. (b) Real [left, dark-green (gray)] and imaginary (right, black) part of the energy spectrum of the chain of $N = 12$ sites with $u = v/w = 2/3$ vs the gain-loss contrast γ. The energy E is in units of w. (c) Magnified view of (b) in the vicinity of $\gamma_{cr} \ll |v - w|$ where the edge-state eigenvalues collapse to an exceptional point of Eq. (20).

III. $\mathcal{PT}$-SYMMETRIC SSH MODEL

We now consider a $\mathcal{PT}$-symmetric extension of the SSH model governed by the non-Hermitian Hamiltonian,

$$\mathcal{H}_{\mathcal{PT}} = \mathcal{H} + i\gamma \sum_{n=1}^{N} (-1)^{(n-1)}\, |n\rangle\,\langle n|\,, \tag{13}$$

where $\gamma > 0$ is the alternating gain and loss rate on the successive lattice sites as shown schematically in Fig. 2(a). The gain-loss contrast γ determines whether the $\mathcal{PT}$ symmetry is manifest in the real (Hermitian-like) spectrum or is spontaneously broken [21]. In contrast to the Hermitian Hamiltonian $\mathcal{H}$, the Hamiltonian (13) does not respect chiral symmetry but possesses pseudo-anti-Hermiticity, $\{\Sigma_z\mathcal{T}, \mathcal{H}_{\mathcal{PT}}\} = 0$, where $\mathcal{T}$ denotes complex conjugation that here coincides with the time-reversal operator. By construction, $\mathcal{H}_{\mathcal{PT}}$ respects parity-time symmetry $[\hat{\mathcal{PT}}, \mathcal{H}_{\mathcal{PT}}] = 0$, where $\hat{\mathcal{PT}}$ is the $\mathcal{PT}$-symmetry operator with $\mathcal{P}$ represented by the backward identity (exchange) matrix. The combined effect of these two symmetries leads to a spectrum symmetric with respect to both the real and the imaginary axis $E \to E^*$ and $E \to -E^*$.

A. Bulk states

The bulk k-space Hamiltonian is now given by

$$\mathcal{H}_{\mathcal{PT}}(k) = \begin{pmatrix} i\gamma & v + we^{-ik} \\ v + we^{ik} & -i\gamma \end{pmatrix}, \tag{14}$$

with the dispersion relation,

$$E(k) = \pm\sqrt{v^2 + w^2 + 2vw\cos k - \gamma^2}, \tag{15}$$

that leads to the $\mathcal{PT}$ classification for the bulk states of the system based on whether all, some, or none of the eigenvalues are real. The corresponding $\mathcal{PT}$ phases are

$$\begin{aligned} \gamma &< |v-w|, \quad \text{unbroken}, \\ |v-w| < \gamma &< |v+w|, \quad \text{partially broken}, \\ \gamma &> |v+w|, \quad \text{fully broken}, \end{aligned} \tag{16}$$

which holds in the thermodynamic limit $N \to \infty$. Observe in Fig. 2(b) that, for short lattices ($N \sim 10$) with few eigenstates, the partially and fully $\mathcal{PT}$-broken phases of the bulk occur for the values of gain-loss contrast $|v-w| < \gamma < |v+w|$ [31].

It has been shown [23,24] that as long as a bulk band gap exists, the topological properties of this system can be deduced again by a winding number of the same form as in the Hermitian case Eq. (4). Hence, the system is topologically nontrivial for $w > v$ (such that $\mathcal{W} \neq 0$) and $\gamma < |v-w|$ (open gap) or, equivalently, for $w > \gamma + v$.

B. Edge states

We now discuss the properties of the edge states in finite lattices with the topologically nontrivial configuration. Note that for any finite system with nontrivial topology the edge-state eigenvalues collapse to an exceptional point at a small critical value of $\gamma_{cr} \ll |v-w|$ as seen in Fig. 2(c). Our main goal is to determine the value of γ_{cr} at which the edge states attain an exceptional point with zero energy and then acquire imaginary energy eigenvalues. To construct an effective two-state Hamiltonian $\mathcal{H}^{(\mathrm{eff})}_{\mathcal{PT}}$, we use the same wave-function ansatz of Eqs. (7) for the edge-states $|L, R\rangle$ and find that

$$\mathcal{H}_{\mathcal{PT}}\,|L, R\rangle = \mathcal{H}\,|L, R\rangle \pm i\gamma\,|L, R\rangle\,. \tag{17}$$

Since $\mathcal{H}\,|L, R\rangle = 0$ for $N \to \infty$, the above relation reveals that the two states are also eigenstates of $\mathcal{H}_{\mathcal{PT}}$ in the thermodynamic limit but with the corresponding imaginary eigenvalues $\pm i\gamma$. This suggests that the ansatz (7) is indeed suitable for the non-Hermitian case as well. It is then easy to see that the diagonal elements (imaginary potential) in

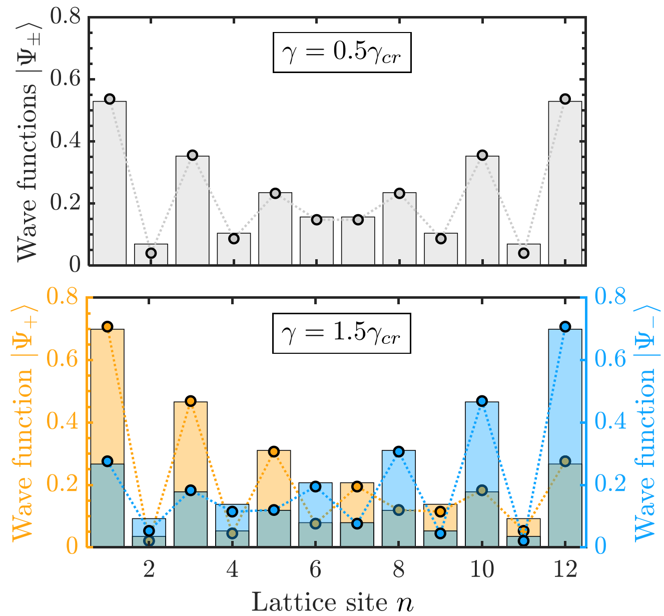

FIG. 3. Spatial profile of the eigenstates $|\Psi_\pm\rangle$ (absolute values of the amplitudes at lattice sites n) for γ smaller (upper panel) and larger (lower panel) than γ_{cr}. Bars correspond to the analytical Eq. (22) with $|L, R\rangle$ of Eqs. (7) and the filled circles connected by dotted lines show the exact numerical results.

Eq. (13) will translate to diagonal elements $\mathcal{E}_{L,R} = \pm i\gamma$ of the effective Hamiltonian but will not affect the off-diagonal elements of $\mathcal{H}^{(\mathrm{eff})}_{\mathcal{PT}}$. Hence, the effective Hamiltonian is

$$\mathcal{H}^{(\mathrm{eff})}_{\mathcal{PT}} = \begin{pmatrix} i\gamma & C \\ C & -i\gamma \end{pmatrix}, \tag{18}$$

with C given in Eq. (10). The eigenvalues of $\mathcal{H}^{(\mathrm{eff})}_{\mathcal{PT}}$ are given by

$$E_\pm = \pm\sqrt{C^2 - \gamma^2}, \tag{19}$$

and the critical value of the gain-loss contrast γ_{cr} at which the eigenvalues of the hybridized edge states are expected to turn from real to imaginary is

$$\gamma_{cr} = |C| = v\,\frac{1-u^2}{1-u^N}\,u^{(N/2-1)}. \tag{20}$$

In Fig. 2(c) we show the magnified spectrum of the system in the vicinity of γ_{cr} obtained from exact diagonalization of the full Hamiltonian (13) and compare it with the analytical prediction of Eq. (19), revealing an excellent agreement.

The eigenstates of the effective Hamiltonian (18) corresponding to the eigenvalues $E_\pm$ are again given by linear superpositions of the edge-state $|L, R\rangle$,

$$\begin{aligned} |\Psi_+\rangle &= \frac{1}{\sqrt{\mathcal{N}}}(\cos\theta\,|L\rangle + \sin\theta\,|R\rangle), \\ |\Psi_-\rangle &= \frac{1}{\sqrt{\mathcal{N}}}(\sin\theta\,|L\rangle - \cos\theta\,|R\rangle), \end{aligned} \tag{21}$$

where $\theta \equiv \frac{1}{2}\tan^{-1}\left(\frac{C}{i\gamma}\right) = -\frac{i}{4}\ln\frac{\gamma+C}{\gamma-C}$ is the complex mixing angle and $\mathcal{N}$ is a normalization constant. In Fig. 3 we show the wave-functions $|\Psi_\pm\rangle$ for two values of γ below and above the

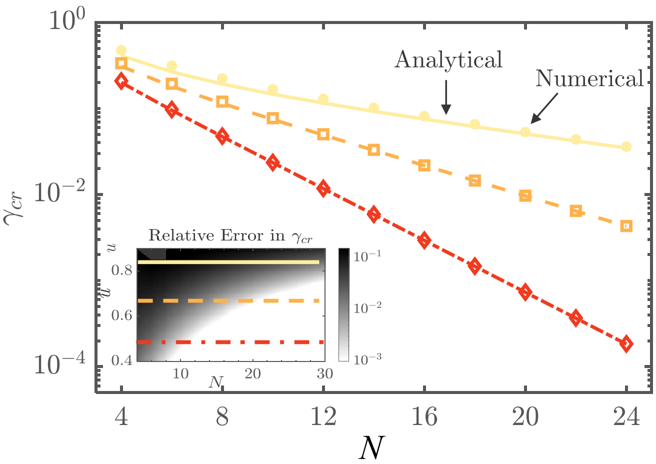

FIG. 4. Critical values of the gain-loss contrast γ_{cr} (in units of w) vs the lattice length M for three different values of $u = v/w = 5/6, 2/3, 1/2$. Main panel shows the comparison between the analytical expression (20) (solid yellow, dashed orange, and dashed-dot red lines) and the exact numerical values (circles, squares, and diamonds). The inset shows the relative error in γ_{cr} of Eq. (20) vs M and u with the horizontal lines corresponding to the three values of u used in the main panel.

$\mathcal{PT}$-symmetry breaking point $\gamma_{cr} = |C|$. Note that below or at the exceptional point $\gamma \leqslant |C|$, the eigenstates of $\mathcal{H}^{(\text{eff})}_{\mathcal{PT}}$ have equal contributions from both edge-states $|\langle L, R|\Psi_\pm\rangle| = 1/\sqrt{2}$, similar to the Hermitian case of Eq. (12); whereas above the exceptional point, $\gamma > |C|$, states $|\Psi_\pm\rangle$ have increasingly larger contributions from $|L, R\rangle$, respectively, as expected. In the limit of $\gamma \gg |C|$, the edge states completely decouple and the eigenstates of the effective Hamiltonian (18) reduce to the edge states $|\Psi_\pm\rangle \to |L, R\rangle$ with purely imaginary energy eigenvalues $E_\pm \to \pm i\gamma$, respectively.

In Fig. 4 we compare the analytical prediction of Eq. (20) with the values of γ_{cr} obtained by exact diagonalization of the full Hamiltonian (13) for different N and $u = v/w$ and extraction of the exceptional points. We find nearly perfect agreement between the analytical and numerical results for sufficiently small $u \lesssim 2/3$ and only small discrepancy for larger u and small N. Note, finally, that, according to Eq. (20), γ_{cr} decreases exponentially with increasing the system size N and, hence, for sufficient large N the exceptional point for the edge state eigenvalues occurs already in the close vicinity of $\gamma = 0$.

IV. $\mathcal{PT}$-SYMMETRIC SSH MODEL WITH ARBITRARY GAIN AND LOSS

With minor modifications, the effective description of the edge states presented above can be applied to a larger variety of systems with arbitrary gain and loss rates with the only restrictions being that they must respect the global $\mathcal{PT}$ symmetry whereas retaining the bulk energy gap. We, therefore, consider once again an SSH chain with alternating gain and loss rates γ_n on the successive sites, as described by the Hamiltonian,

$$\tilde{\mathcal{H}}_{\mathcal{PT}} = \mathcal{H} + i\sum_{n=1}^{N}(-1)^{(n-1)}\gamma_n\,|n\rangle\,\langle n|\,, \tag{22}$$

where $\mathcal{H}$ is the Hamiltonian of Eq. (1), whereas the global $\mathcal{PT}$ symmetry requires that

$$\gamma_n = \gamma_{N-n+1}. \tag{23}$$

We again construct an effective two-state Hamiltonian for the edge states $|L, R\rangle$ of Eqs. (7). As before, the off-diagonal elements of the effective Hamiltonian remain the same $\langle L|\tilde{\mathcal{H}}_{\mathcal{PT}}|R\rangle = \langle R|\tilde{\mathcal{H}}_{\mathcal{PT}}|L\rangle^* = C$, whereas for the diagonal elements and we have

$$\mathcal{E}_L \equiv \langle L|\tilde{\mathcal{H}}_{\mathcal{PT}}|L\rangle = i\sum_{n=1}^{N}(-1)^{(n-1)}\gamma_n\left|c_n^L\right|^2$$
$$= i\bar{\gamma}, \tag{24a}$$
$$\mathcal{E}_R \equiv \langle R|\tilde{\mathcal{H}}_{\mathcal{PT}}|R\rangle = i\sum_{n=1}^{N}(-1)^{(n-1)}\gamma_n\left|c_n^R\right|^2$$
$$= -i\bar{\gamma}, \tag{24b}$$

where

$$\bar{\gamma} \equiv \frac{\sum_{n=1}^{N/2}\gamma_{2n-1}u^{2(n-1)}}{\sum_{n=1}^{N/2}u^{2(n-1)}} \tag{25}$$

is the effective gain and loss rate for states $|L\rangle$ and $|R\rangle$, respectively. Hence, the effective Hamiltonian is

$$\tilde{\mathcal{H}}^{(\text{eff})}_{\mathcal{PT}} = \begin{pmatrix} i\bar{\gamma} & C \\ C & -i\bar{\gamma} \end{pmatrix}, \tag{26}$$

with the eigenvalues (19) and eigenvectors (22) with the replacement $\gamma \to \bar{\gamma}$. The critical value of $\bar{\gamma}$ at which the edge states attain an exceptional point are $\bar{\gamma}_{cr} = |C|$.

To verify our analytical predictions for the general model in Eq. (22), we consider three different spatial distributions of the complex potential $\gamma_n \in [0, U]$ for $n = 1, 2, \ldots, N/2$,

$$\gamma_n = U\frac{N/2 - n}{N/2 - 1}, \tag{27a}$$
$$\gamma_n = U\frac{n-1}{N/2 - 1}, \tag{27b}$$
$$\gamma_n = U r_n, \tag{27c}$$

which satisfy Eq. (23) for $n = N/2 + 1, N/2 + 2, \ldots, N$. Here case (a) corresponds to γ_n linearly decreasing from the edges to the center of the chain; case (b) corresponds to γ_n linearly increasing from edge to center; and case (c) corresponds to arbitrary γ_n with $r_n \in [0, 1]$ being uniformly distributed random numbers as we illustrate in the top panels of Fig. 5. In the middle panels of Fig. 5 we plot the critical values of $\bar{\gamma}_{cr}$ at which the edge-state eigenvalues collapse to an exceptional point as predicted analytically $\bar{\gamma}_{cr} = |C|$ and obtained numerically via exact diagonalization of the full Hamiltonian (22) for different N's and $u = v/w$'s. In all cases, we find good agreement between the analytical and the numerical calculations. The largest deviation between the analytical and the numerical values of $\bar{\gamma}_{cr}$ are obtained for $u \gtrsim 2/3$ and small $N \lesssim 10$

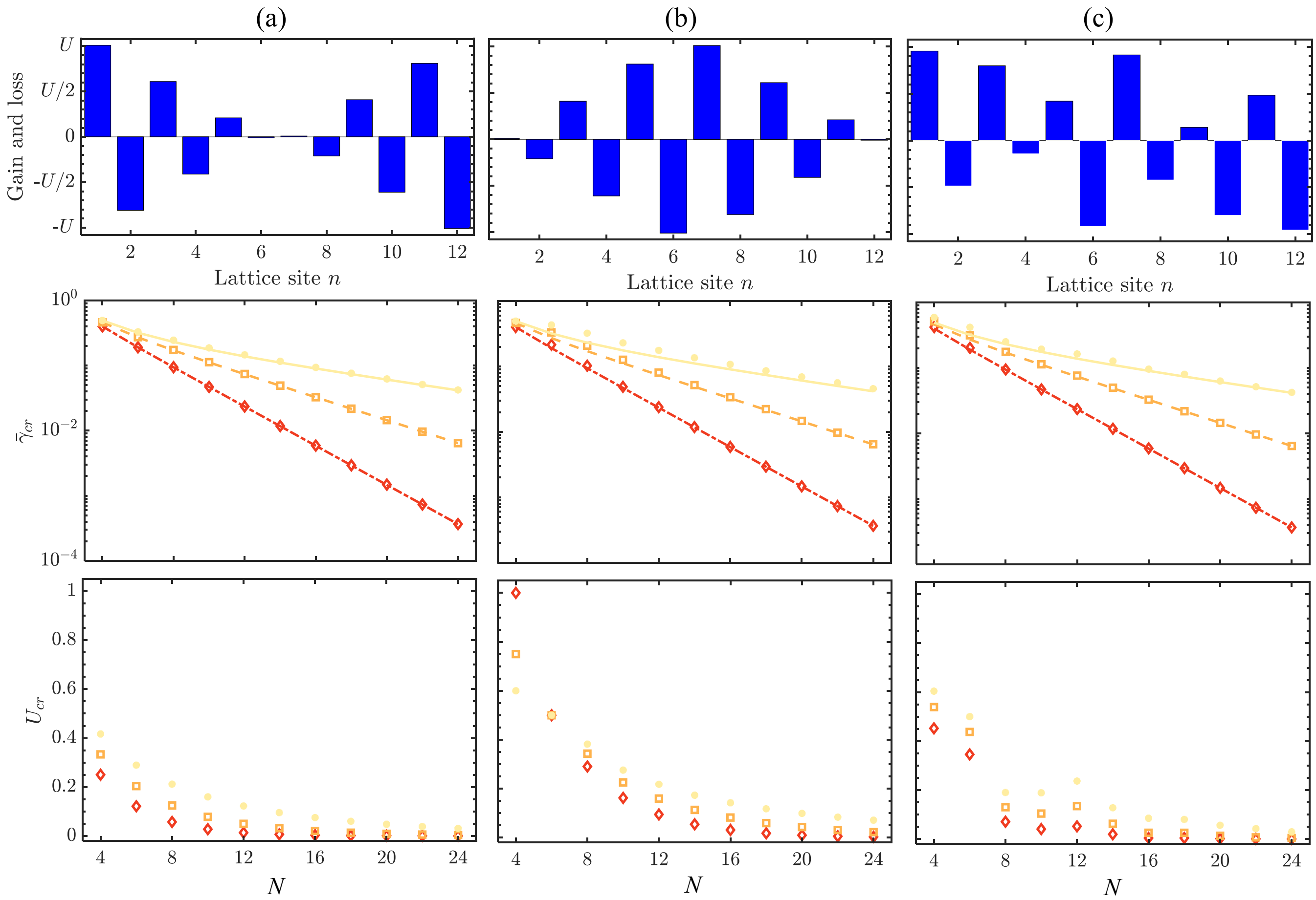

FIG. 5. $\mathcal{PT}$-symmetry breaking in SSH chains with arbitrary gain and loss. Top panels illustrate the three different imaginary potentials for the Hamiltonian (22) given by Eqs. (27a)–(27c), respectively. Middle panels show the critical values of $\bar{\gamma}_{cr}$ (in units of w) vs the chain length N for $u = w/v = 5/6, 2/3, 1/2$ (same line and symbol styles and color code as in Fig. 4) obtained numerically (symbols) and analytically (lines). Bottom panels shown the critical values of the potential amplitudes U (in units of w) in Eqs. (27) that correspond to $\bar{\gamma}_{cr}$ in the middle-panel plots.

especially for case (b) with the maximum of the potential in the middle of the chain $\gamma_{N/2} = U$. In the bottom panels of Fig. 5 we show the values of $U = U_{cr}$ corresponding to the exceptional points ($\bar{\gamma} = \bar{\gamma}_{cr}$) obtained from the numerical simulations. U_{cr} is largest for case (b) since the wave functions of the edge states that decay away from the boundaries are less affected by the stronger imaginary potential in the middle of the chain. Now the potential in the vicinity of $n = N/2$ can take large values $\gamma_n \sim |w - v|$, comparable to the bulk gap. But the strong potential in the middle of the chain significantly affects the spectrum of the bulk which, in turn, can perturb the zero-energy edge states. This explains the largest deviation between the analytically predicted and numerically calculated values of $\bar{\gamma}_{cr}$ for case (b) with large u and small N for which the edge-state wave functions have relatively large amplitudes at the middle of the chain.

V. CONCLUSIONS

To summarize, we have studied the single-particle non-Hermitian, $\mathcal{PT}$ SSH model in the topologically nontrivial configuration and derived an effective analytical model for the edge states in finite lattices. Our effective model accounts for the evanescent coupling between the edge states, accurately describes their properties, and gives physically transparent interpretation for the $\mathcal{PT}$-symmetry breaking for the edge states, which we verified by exact numerical calculations.

Our effective model neglects the interaction between the edge and the bulk states. It is, therefore, valid when the coupling C between the edge states is sufficiently smaller than the gap separating them from the bulk states $|C| \ll |v - w|$ since otherwise the hybridized edge levels will approach the bulk levels and their interactions cannot be neglected. Since the bulk gap is closing when $u = v/w \to 1$, whereas the coupling between the edge states, and thereby their splitting $|C| \propto u^{N/2}$ is stronger for shorter lattice length N, our approach yields accurate results for sufficiently small $u < 1$ and large $N > 10$. For larger u and/or smaller N, inclusion of perturbative corrections due to the interaction of the edge states with the bulk states will become necessary for obtaining accurate results.

The studied model is experimentally relevant as the ordered and disordered non-Hermitian Hamiltonians (13) and (22) can be physically implemented by the addition of alternating optical gain and loss in a lattice of coupled optical elements, such as waveguides or cavities that have been realized in a number of recent experiments [25,27]. As an extension of the present ppaper, it would be interesting to consider topologically nontrivial interfaces between finite SSH sublattices and explore the resulting localized zero-energy modes and their effective couplings for robust quantum information storage and transfer purposes. Another interesting research direction could be to develop effective models for higher-order edge states in multidimensional topological systems [47].

ACKNOWLEDGMENT

A.F.T., N.E.P. and D.P. were supported by the EU QuantERA Project PACE-IN (GSRT Grant No. T11EPA4-00015).

[1] D. J. Thouless, M. Kohmoto, M. P. Nightingale and M. den Nijs, Phys. Rev. Lett. **49**, 405 (1982).
[2] K. von Klitzing, Rev. Mod. Phys. **58**, 519 (1986).
[3] X. G. Wen, Adv. Phys. **44**, 405 (1995).
[4] M. Z. Hasan and C. L. Kane, Rev. Mod. Phys. **82**, 3045 (2010).
[5] X. L. Qi and S. C. Zhang, Rev. Mod. Phys. **83**, 1057 (2011).
[6] A. Y. Kitaev, Phys.-Usp. **44**, 131 (2001).
[7] M. König *et al.*, Science **318**, 766 (2007).
[8] C. Nayak, S. H. Simon, A. Stern, M. Freedman, and S. Das Sarma, Rev. Mod. Phys. **80**, 1083 (2008).
[9] D. Pesin and A. H. MacDonald, Nature Mater. **11**, 409 (2012).
[10] F. D. M. Haldane and S. Raghu, Phys. Rev. Lett. **100**, 013904 (2008).
[11] Z. Wang, Y. D. Chong, J. D. Joannopoulos and M. Soljačić, Phys. Rev. Lett. **100**, 013905 (2008).
[12] M. C. Rechtsman *et al.*, Nature (London) **496**, 196 (2013).
[13] L. Lu, J. D. Joannopoulos and M. Soljačić, Nat. Photonics **8**, 821 (2014).
[14] T. Ozawa, Rev. Mod. Phys. **91**, 015006 (2019).
[15] Z. Chen and D. Leykam, Light Sci. Appl. **9**, 203 (2020).
[16] K. G. Makris, R. El-Ganainy, D. N. Christodoulides, and Z. H. Musslimani, Phys. Rev. Lett. **100**, 103904 (2008).
[17] S. Klaiman, U. Günther, and N. Moiseyev, Phys. Rev. Lett. **101**, 080402 (2008).
[18] C. E. Rüter *et al.*, Nat. Phys. **6**, 192 (2010).
[19] R. El-Ganainy *et al.*, Nat. Phys. **14**, 11 (2018).
[20] Ş. K. Özdemir, S. Rotter, F. Nori, and L. Yang, Nature Mater. **18**, 783 (2019).
[21] C. M. Bender and S. Boettcher, Phys. Rev. Lett. **80**, 5243 (1998).
[22] Y. C. Hu and T. L. Hughes, Phys. Rev. B **84**, 153101 (2011).
[23] K. Esaki, M. Sato, K. Hasebe, and M. Kohmoto, Phys. Rev. B **84**, 205128 (2011).
[24] H. Schomerus, Opt. Lett. **38**, 1912 (2013).
[25] J. M. Zeuner, M. C. Rechtsman, Y. Plotnik, Y. Lumer, S. Nolte, M. S. Rudner, M. Segev, and A. Szameit, Phys. Rev. Lett. **115**, 040402 (2015).
[26] L. Xiao *et al.*, Nat. Phys. **13**, 1117 (2017).
[27] S. Weimann *et al.*, Nature Mater. **16**, 433 (2017).
[28] V. M. Martinez Alvarez, J. E. Barrios Vargas, M. Berdakin, and L. E. F. Foa Torres, Eur. Phys. J.: Spec. Top. **227**, 1295 (2018).
[29] M. Pan, H. Zhao, P. Miao, S. Longhi, and L. Feng, Nat. Commun. **9**, 1 (2018).
[30] K. Kawabata, Y. Ashida, H. Katsura, and M. Ueda, Phys. Rev. B **98**, 085116 (2018).
[31] W. Song, W. Sun, C. Chen, Q. Song, S. Xiao, S. Zhu, and T. Li, Phys. Rev. Lett. **123**, 165701 (2019).
[32] S. Xia *et al.*, Science **372**, 72 (2021).
[33] A. Stegmaier, S. Imhof, T. Helbig, T. Hofmann, C. H. Lee, M. Kremer, A. Fritzsche, T. Feichtner, S. Klembt, S. Höfling, I. Boettcher, I. C. Fulga, L. Ma, O. G. Schmidt, M. Greiter, T. Kiessling, A. Szameit, and R. Thomale, Phys. Rev. Lett. **126**, 215302 (2021).
[34] Q. Y. Xu, F. Liu, C. Z. Chen, and D. H. Xu, Phys. Rev. B **105**, 075411 (2022).
[35] H. Zhao *et al.*, Science **365**, 1163 (2019).
[36] S. Weidemann *et al.*, Science **368**, 311 (2020).
[37] G. Harari *et al.*, Science **359**, eaar4003 (2018).
[38] M. A. Bandres *et al.*, Science **359**, eaar4005 (2018).
[39] M. Parto, Phys. Rev. Lett. **120**, 113901 (2018).
[40] O. Bendix, R. Fleischmann, T. Kottos, and B. Shapiro, Phys. Rev. Lett. **103**, 030402 (2009).
[41] I. V. Barashenkov, L. Baker, and N. V. Alexeeva, Phys. Rev. A **87**, 033819 (2013).
[42] D. E. Pelinovsky, D. A. Zezyulin, and V. V. Konotop, J. Phys. A: Math. Theor. **47**, 085204 (2014).
[43] J. K. Asbóth, L. Oroszlány, and A. Pályi, Lecture Notes Phys. **919**, 166 (2016).
[44] N. K. Efremidis, Phys. Rev. A **104**, 053531 (2021).
[45] X. R. Wang, C. X. Guo, and S. P. Kou, Phys. Rev. B **101**, 121116(R) (2020).
[46] L. J. Lang, Y. Wang, H. Wang, and Y. D. Chong, Phys. Rev. B **98**, 094307 (2018).
[47] M. Ezawa, Phys. Rev. Lett. **120**, 026801 (2018).